

Supplementary Information

Sharpening surface of magnetic paranematic droplets†

Alexander Tokarev,^a Wah-Keat Lee,^b Igor Sevonkaev,^c Dan Goia,^c Konstantin G. Kornev ^{*a}

^a*Department of Materials Science and Engineering, 161 Surrine Hall, Clemson University, Clemson, SC*

29634, USA

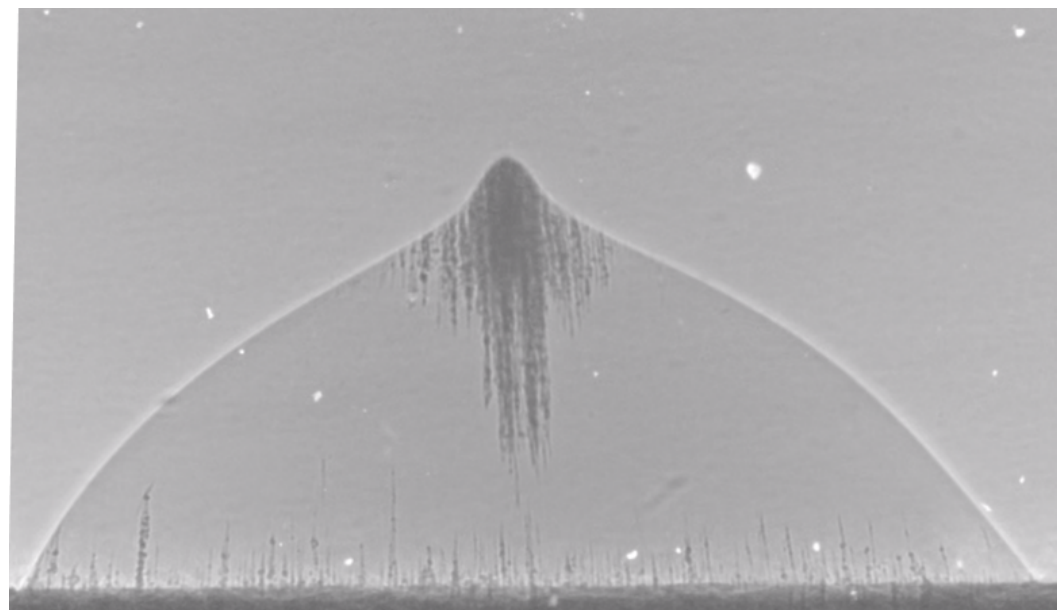
^b*Advanced Photon Source, Argonne National Laboratory, Argonne, IL 60439, USA*

^c*Center for Advanced Materials Processing, Clarkson University, Potsdam, New York 13699, USA*

^{*}kkornev@clemson.edu

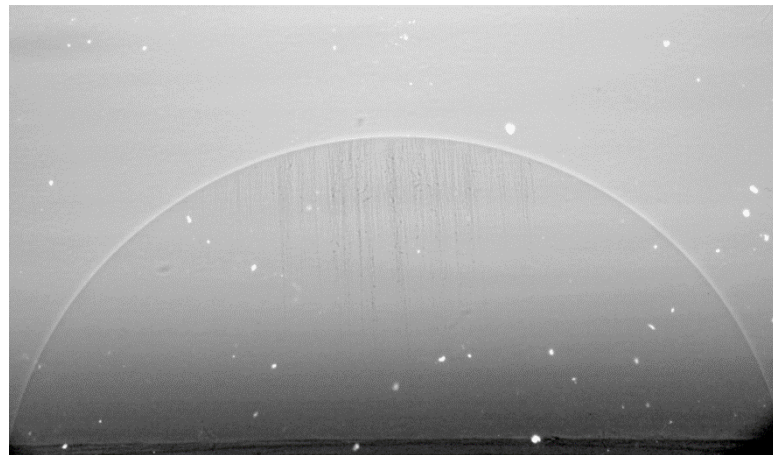
Video S1

This video shows nanorod ordering and clustering leading to the changes of droplet shape when the magnet moves towards the drop.



Video S2

This video shows the reversibility of the cluster formation. Cluster is formed in magnetic field and when the field is removed, the nanorods and bundles of nanorods spread apart and finally disappear due to thermal excitations.



Analysis of droplet shape.

When a droplet is sitting on a wire it forms contact angle β with the wire surface (Fig. 3c in the main manuscript). In order to fit the droplet shape, we used the first integral of the Laplace equation of capillarity¹

$$-\frac{df}{dr} = \frac{r^2(x_2 - x_1 \cos \beta) + x_1 x_2 (x_2 \cos \beta - x_1)}{\left[r^2(x_2 - x_1 \cos \beta)^2(x_2^2 - r^2) - x_1^2(x_2 \cos \beta - x_1)^2(x_2^2 - r^2) \right]^{\frac{1}{2}}} \quad (\text{S1})$$

The image analysis was conducted using MatLab and numerically solving equation (S1). The droplet radius, x_2 , and wire radius, $x_1 = 0.23$ mm were taken from the images. Two other parameters, L , and β were adjusted to fit the image with function f , a solution to equation (S1).

For droplets with cusped poles, one can introduce a radius of equivalent wire, x_1 , as follows. In the cusp, we introduce the cone radius r as shown in Fig. 6 b,c: we drew a horizontal line emanating from the outmost dark edge of the magnetic cluster and measure the radius as the distance between the center axis and this outmost dark edge. This line and associated circular disk was considered as the bottom boundary of the poppy head. With this definition of the cone radius, we found the ratio $r/x_1 = 2.7$ for the droplet in Fig. 3b,c. In order to check if the r/x_1 - ratio is universal for all poppy heads, we conducted the X-ray imaging experiments with different droplets having different concentrations of nanorods. Upon application of magnetic field, these droplets generated different cusps with the cone radii r_1 , r_2 and r_3 (Fig. S1a-c). Then we calculated the radius of the equivalent wire for the first droplet x_{11} as $r_1/2.7$ (Fig. S1a). Using this apparent wire radius, we adjusted two other parameters of unduloid, L_1 , and β_1 , to fit the image with function $z(r)$, a solution to equation (S1). Analyzing two other droplets with smaller nanorod concentrations, we kept the L -parameter same (as that obtained for the first droplet), and introduced the equivalent wire radii as $x_{12} = r_2/2.7$ and $x_{13} = r_3/2.7$ and adjusted angle β to fit these two images with functions $z(r)$. The corresponding contact angles were obtained as $\beta_1 = 49.4^\circ$, $\beta_2 = 49.1^\circ$, $\beta_3 = 49.3^\circ$.

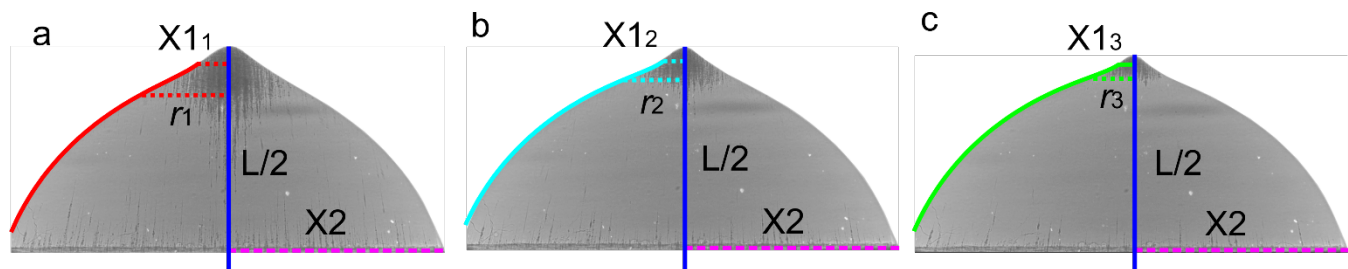


Figure S1. X-ray images of droplets with 3 different initial concentrations of nanorods showing the same ratio $r_1/x_{11} = r_2/x_{12} = r_3/x_{13} = 2.7$

Figure S1 confirms that the numerical solutions of equation (S1) provide the perfect fit to the experimental results. Therefore, we conclude that the droplets with the same radius (X_2) and different radii of the magnetic cones can be described by an unduloidal solution of equation (S1) by choosing an apparent wire radius as $X_1 = r/2.7$ and adjusting cone angle β keeping the same L-parameter for all droplets.

Applying this procedure, we analyzed seven droplets of the same size $X_2 = 2.23 \pm 0.2\text{mm}$ forming the poppy heads. An arbitrary chosen droplet was used to adjust the L-parameter. To fit the profiles of other six droplets, the L-parameter was not changed anymore, only contact angle β was varied to find the best fit. The average cone angle β was then reported.

Universality of the cone angle

In Fig. 3 in the main manuscript we show the hysteresis loop taken on a piece of alumina membrane before its dissolution. The measurements were conducted on the 2900-02C Alternating Gradient Magnetometer (Princeton Measurements Corp.). A linear part of the magnetization curve emanating from zero (Fig. 3b) confirms that as-synthesized nickel nanorods do not possess any permanent magnetic moment, i.e. their magnetic behavior in the milliTesla fields can be described by a linear constitutive equation for magnetization, $\mathbf{m} = \mu_0\chi \mathbf{H}$, or taking into account the sample volume V , we write this equation as $mV = k\mu_0 H$ with the measured proportionality constant $k=0.00019$. Then the susceptibility was obtained as $\chi = m/H = k\mu_0/V = 48$. Therefore, the susceptibility constant appears much greater than one, $\chi \gg 1$ and we will take advantage of this large parameter by describing the cusp asymptotically.

The center of the spherical polar coordinates is placed at the cone vertex with polar angle $\theta=0$ taken at the cone axis. We assume that the gap separating the driving magnet from the vertex is much larger than the size of the poppy head. Therefore, the problem is reduced to an analysis of possible cone-like

configurations of the poppy head where the opening angle 2β is unknown. This approximation corresponds to the inner expansion of the matched asymptotic expansion of the general solution described in Ref.². According to Fig. 1a, magnetic field of the inner expansion has to grow at infinity.

It is convenient to describe the field distribution in terms of magnetostatic potential φ , $\mathbf{H} = -\nabla\varphi$. This potential φ must satisfy the Laplace equation inside and outside the magnetic cone, $\Delta\varphi=0$. At infinity the field is allowed to be singular. At the surface of liquid cone the potential is continuous, $\varphi^{\text{air}} = \varphi^{\text{liquid}}$, but its normal derivative is not. Using the continuity condition for the magnetic induction vector, $B_n^{\text{air}} = B_n^{\text{liquid}}$, the boundary condition for the normal derivatives is written as $\partial\varphi^{\text{air}}/\partial n = (1+\chi)\partial\varphi^{\text{liquid}}/\partial n$.

In magnetic cones, the susceptibility is large, $\chi \gg 1$, therefore, we can seek an asymptotic solution to this problem as $\varphi = \varphi_0 + \varphi_1/(1+\chi) + \varphi_2/(1+\chi)^2 + \dots$ In the zero approximation, the boundary condition for the normal derivative gives: $\partial\varphi_0^{\text{liquid}}/\partial n = 0$. The solution to Laplace equation in the cone with the zero normal derivative at its surface is a constant, $\varphi_0^{\text{liquid}} = \Phi$. Therefore, for the cone exterior, we have to find a solution of the Laplace equation growing at infinity satisfying the remaining boundary condition at the cone surface, $\varphi_0^{\text{air}} = \varphi_0^{\text{liquid}} = \Phi$. Thus, the problem for the inner expansion is reduced to the Taylor problem of a liquid cone subject to external electric field where the electric field is replaced by the magnetic field and dielectric constant is replaced by the permeability $(1+\chi)^3$. As shown by Taylor, to balance the capillary pressure at the cone surface, the Maxwell stress has to depend on the radial polar coordinate R as $T \sim 1/R$. Therefore, the magnetostatic potential has to have the following radial dependence $\varphi_0 \sim R^{1/2}$. Using these arguments, we reproduce the Taylor solution, $\varphi_0^{\text{air}} = \Phi + A R^{1/2} P_{1/2}(\cos\theta)$, where $P_{1/2}$ is the Legendre function of the order of $\frac{1}{2}$. The cone surface $\theta = \theta_0$ can be made equipotential only if the Legendre function becomes zero, $P_{1/2}(\cos\theta_0) = 0$. This condition specifies the angle $\theta_0 = 130.7^\circ$. Thus, the cusp is enveloped by the Taylor cone with its half-angle $\beta=49.3^\circ$ ³. Our experimental data confirm this result.

Effect of gravity

The gravitational force is written as $F_g = mg$. Taking the poppy head volume as the volume of a cone

with radius r and height h , $V = \frac{1}{3}\pi r^2 h = \frac{1}{3}\pi r^3 \tan \beta$, we obtain the following ratio

$$\frac{F_g}{F_w} = \frac{\pi r^3 \tan \beta \cdot \rho g}{6\pi r \sigma \cos(\beta)} = \frac{r^2 \tan \beta \cdot \rho g}{6\sigma \cos(\beta)}.$$

For a cusp with the greatest measured radius $r = 1\text{mm}$, this ratio is estimated as ~ 0.1 . Therefore, the gravitational force is an order of magnitude lower than the surface tension force. Therefore, the effect of gravity can be safely neglected.

Synthesis of spherical Ni nanoparticles

Spherical single crystal and highly crystalline uniform Ni nanoparticles of different sizes were obtained via reduction of the nickel carbonate basic salt (The Shepherd Chemical Company) in high quality grade di-ethylene glycol (99.99% DEG). The polyol served as a reducing and dispersing agent, and as a medium. Final size of nickel particles was controlled by the limited seeding mechanism described recently^{4, 5}. Based on that method, dispersions with the particles of diameter $d=30\pm6.1$, 165 ± 27.2 , and $605\pm69.5\text{ nm}$ were produced (Fig. 4).

The extracted particles were washed repeatedly with acetone and water, dried, and inspected by field emission scanning (FESEM, JEOL-7400) and transmission (TEM, JEM- 2010) electron microscopy. Acquired micrographs were analyzed with ImageJ software in order to collect statistics on nickel particle size distribution. For the latter, the particles were assumed to be approximately spherical and for each sample ~ 200 randomly selected crystals were measured. The particles were additionally analyzed by X-ray diffraction (XRD, Bruker-AXS D8 Focus), in order to evaluate the crystal structure and

estimate the length scales over which the crystalline order persists (the crystallite sizes), using the Scherrer's equation⁶.

Shapes of nanobead laden droplets.

Nickel nanoparticles of different sizes were used to investigate the drop deformation and nanoparticle aggregation. Spherical particles of 3 different sizes – 30nm, 165nm and 605nm where synthesized for this study. At high concentration of 30 nm magnetic beads, e.g. 10 wt % concentration in Fig. S2, the entire droplet deforms in magnetic field. Decreasing concentration below 0.2 wt%, one can obtain the cusps. In a series of pictures shown below, 0.2 wt% concentration of nanobeads were used and the cusps were reproduced. In Fig. 6 in the main manuscript we report the critical conditions for the cusps made of nanorods with the same concentration. The time of cusp formation appeared dependent on the nanobead size, Table S1.

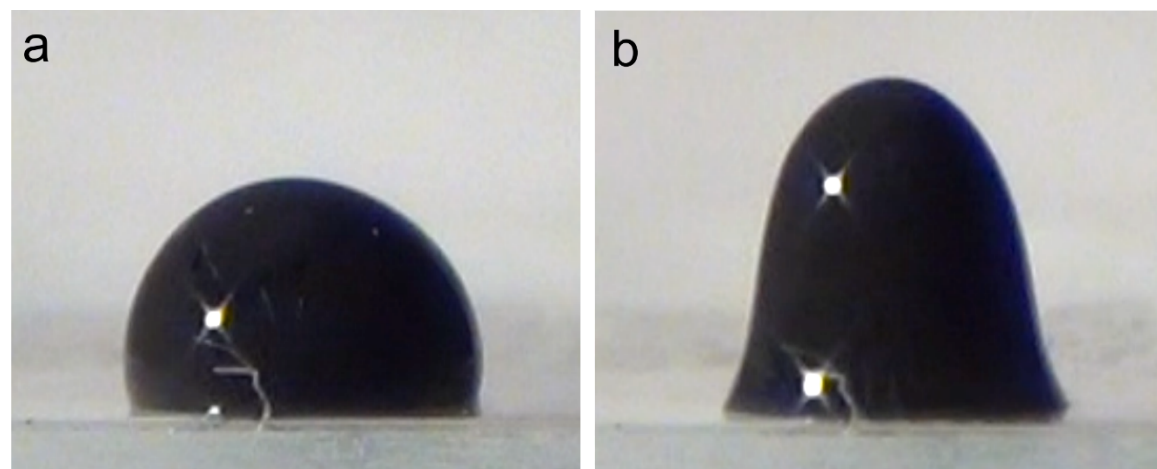


Figure S2. (a) Nanobead laden droplet (10wt%) before application of magnetic field; (b) after application of magnetic field. The entire droplet reacts on the field.

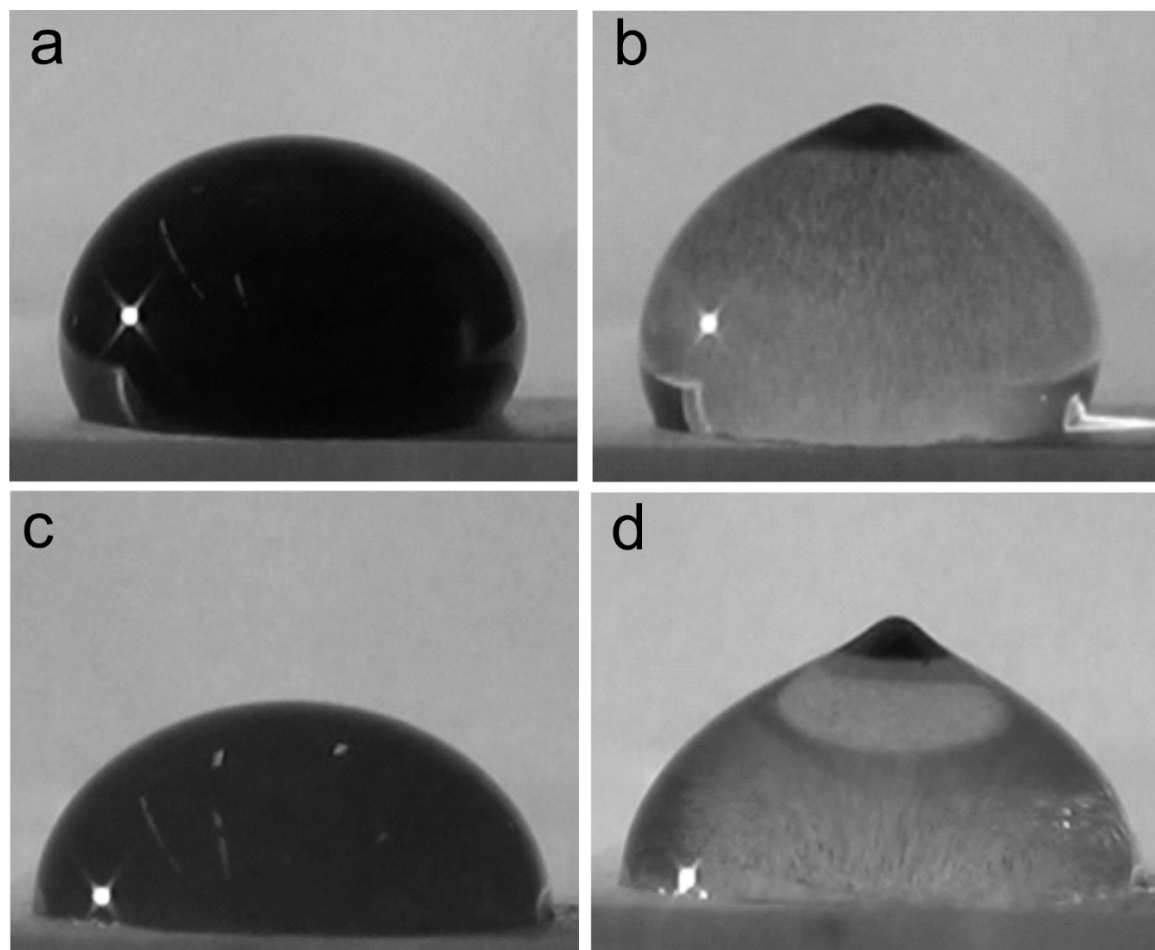


Figure S3. (a) Droplet with 30nm beads (0.2 wt%) before the field application. (b) In the field the droplet shape changes and nanobeads come to the cusp after 70 seconds. (c) Droplet with 165 nm(0.2 wt%) beads before the field application. (d) The same droplet was kept for 11 seconds in the field.

Table S1. Time of the cluster formation for Ni nanoparticles of different size and shape

Sample	Time of the cluster formation (s):
Ni nanorods (200nm in diameter)	2-3
Ni nanospheres (30 nm in diameter)	130
Ni nanospheres (165 nm in diameter)	11
Ni nanospheres (605 nm in diameter)	6

Reversibility of the cluster formation:

Nanorods:

Cluster is formed in magnetic field and when the field is removed, the nanorods and bundles of nanorods spread apart and finally disappear due to thermal excitations.

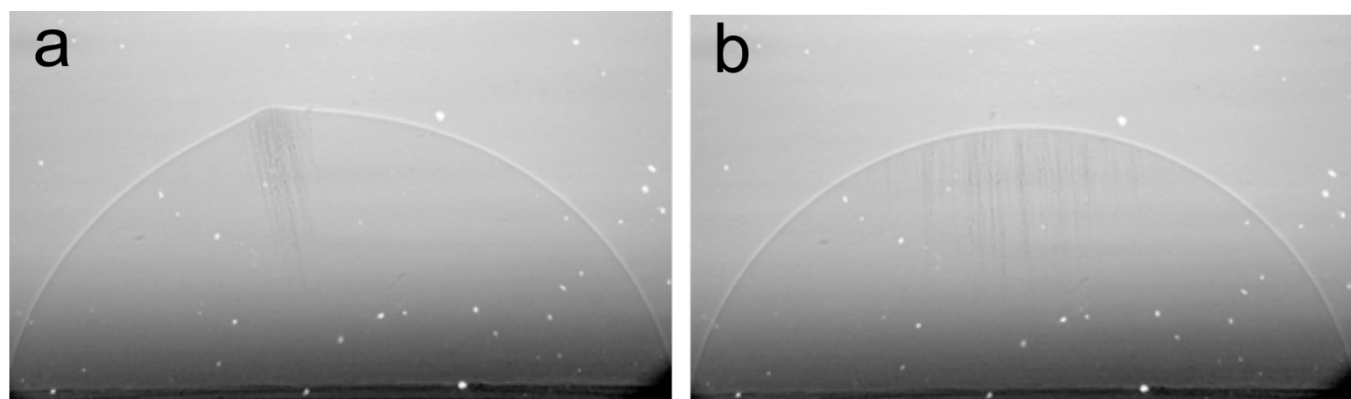


Figure S4. (a) In the field, nanorods come together to form clusters. (b) When the field is removed, the nanorods and bundles of nanorods spread away due to dipole-dipole repulsion. Nanorod concentration is 0.2wt%

In the nanobead laden droplets, the cluster does not disappear completely, it sinks down to the bottom of the droplet. The bundles of chains spread away due to dipole-dipole repulsion, but they do not completely disappear.



Figure S5. Dynamics of cluster settling in the droplet with 100 nm beads of 0.2wt% after the field removal. The time interval between frames is 6 seconds.

References

1. B. J. Carroll, *Journal of Colloid and Interface Science*, 1976, **57**, 488-495.
2. M. Van Dyke, *Perturbation methods in fluid mechanics*, Academic Press, New York, 1964.
3. G. Taylor, *Proceedings of the Royal Society of London Series a- Mathematical and Physical Sciences*, 1964, **280**, 383-397.
4. I. Sevonkaev, V. Privman and D. Goia, *The Journal of Chemical Physics*, 2013, **138**, 014703.
5. D. Goia, M. Lopez and I. Sevonkaev, WO Patent 2,012,123,442, 2012.
6. R. Zsigmondy and P. Scherrer, *Kolloidchemie*, O. Spamer, Leipzig, Germany, 1920.